IEEE Access
Multidisciplinary | Rapid Review | Open Access Journal

Received 1 December 2022, accepted 10 December 2022, date of publication 12 December 2022,
date of current version 20 December 2022.

Digital Object Identifier 10.1109/ACCESS.2022.3228929

RESEARCH ARTICLE

Using the Features Extracted From the Ambient Noise Cross-Correlation Function to Evaluate the Performance of Broadband Seismograph

XUE BAO, FANG YE, HAN ZHANG, AND CHUNWEI JIN
College of Metrology and Measurement Engineering, China Jiliang University, Hangzhou, Zhejiang 310018, China
Corresponding author: Fang Ye (18a0205108@cjlu.edu.cn)

This work was supported by the Zhejiang Provincial Natural Science Foundation of China under Grant LQ20D040002.

ABSTRACT Broadband seismographs are used to collect seismic data over an extended period. Temperature, pressure, and humidity are field variables that can have an impact on the broadband seismograph's performance as well as the accuracy of observational data. Variations in performance, geological structure, and noise source will cause the cross-correlation function of seismic ambient noise to alter. To evaluate the effectiveness of seismographs, we propose to use the whole cross-correlation function as well as the positive and negative time waveforms for feature extraction. The cross-correlation function is decomposed to evaluate the phase variations using Local Mean Decomposition (LMD) and Variational Mode Decomposition (VMD). This is followed by the calculation of the Multivariate Multiscale Fuzzy Entropy Partial Mean (MMFEPM). Wavelet Packet Decomposition (WPD) and MMFEPM are used to evaluate phase variations in the positive and negative time waveforms. WPD combined with Wavelet Feature Scale Entropy (WFSE) is chosen to evaluate the amplitude variations of the cross-correlation function and its positive and negative waveforms. The results show that the proposed methods can identify time offsets within 0.025-2.5s and amplitude variations of 10^{-16}, which provide a new direction for evaluating the performance of seismographs using ambient noise.

INDEX TERMS Broadband seismograph, feature extraction, performance evaluating, ambient noise.

I. INTRODUCTION

Emplacing portable seismic stations has become an essential measure with the development of seismic observation. However, service duration and field uncertainties, such as temperature and humidity [1], [2], [3], emplacement methods [4], [5], geographical conditions [6] and atmospheric pressure [7], [8] may influence the performance of seismographs. As periodic calibration methods can lead to time delays and acquisition interruptions, several methods are proposed to analyze the performance of seismographs in real time using seismic data [9], [10], [11]. Since the seismic data is discontinuous, the seismic ambient noise is selected to evaluate the performance. It can also be evaluated by comparing the short-period ambient noise power spectral density with the long-term noise baseline [12], [13], [14], or by using the data from co-located sensors [15], [16]. The time symmetry analysis of the ambient noise cross-correlation function (NCCF) allows for the separation of the time offsets brought on by the variations of seismograph performance [17], [18], [19]. However, the majority of evaluation methods only process data in the time or frequency domain, which has a negative impact on measurement accuracy. As a result, we analyze the NCCF by feature extraction methods to test the performance variations of the seismograph in the time-frequency domain.

A variety of time-frequency processing methods are chosen to extract the features of NCCF and its positive and negative time waveforms to judge the variations in the performance of seismographs. Empirical Mode Decomposition (EMD) and its improvements, such as Ensemble Empirical Mode Decomposition (EEMD) and Complete Ensemble Empirical Mode Decomposition (CEEMD) are frequently

The associate editor coordinating the review of this manuscript and approving it for publication was Jon Atli Benediktsson.

used for seismic data processing. These methods are based on empirical generalization and temporarily lack mathematical theoretical support. Local Mean Decomposition (LMD) is chosen to perform a preliminary decomposition of NCCF since it can better reflect the detailed characteristics of the seismic signal and avoid the problem of over-decomposition of the seismic signal [20]. VMD performs better in terms of noise robustness than other decomposition methods. It is then utilized as the secondary decomposition to describe the geological features and stratigraphic information in NCCF [21], [22], [23]. Variational Mode Decomposition (VMD) can also be applied to underwater acoustic signals [24], [25]. Wavelet Packet Decomposition (WPD) can adaptively select the corresponding frequency band to match the spectrum according to the signal characteristics. It can improve the time-frequency resolution of seismic signals by taking advantage of time-frequency localization and multi-scale analysis [26]. Positive and negative time waveforms can both have phase information extracted using WPD. As the spatial distribution of noise sources can alter the amplitude of NCCF, WPD is used to extract the amplitude information more pertinently. Following the presentation of the feature extraction methodologies in Section 2, the results are provided in Section 3 and demonstrate the feasibility of the methods using real data in Section 4. Section 5 concludes the phase and amplitude evaluation methods.

II. METHODS

Changes in instrument responses can alter the collected data since it is obtained by convolving the source term, path term, and instrument response. The instrument response function consists of the zero-poles and sensitivity:

$$G(f) = S_d A_0 \frac{\prod_{n-1}^{N} (s - r_n)}{\prod_{m-1}^{M} (s - p_m)} = S_d A_0 H_p(s) \tag{1}$$

where S_d contains all information about the stage's sensitivity, A_0 is the normalization factor, s is a variable in the Laplace transform domain, r_n and p_m are the zeros and poles, respectively.

The performance of seismographs will alter as service time increases and field uncertainty factors, resulting in instrument response parameters changes. The amplitude and phase of the data can be used to assess performance since changes in parameters will have an impact on the data. Variations in zero-poles will influence the amplitude-frequency and phase-frequency responses (Fig. 1), whereas variations in sensitivity will affect the amplitude-frequency response (Fig. 2). The NCCF calculated from the collected ambient noise data is selected to evaluate the performance of the seismograph.

Physical changes in media, seismograph errors, and the spatial distribution of noise sources all have impacts

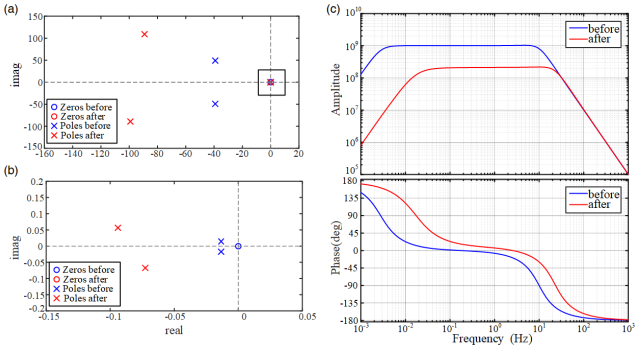

FIGURE 1. The results of zero-poles variations on instrument responses. (a) Variations in zero-poles; (b) Enlargement of the black box in (a); (c) Variations in amplitude-frequency and phase-frequency responses. The results before and after changing the parameters are shown in blue and red, respectively.

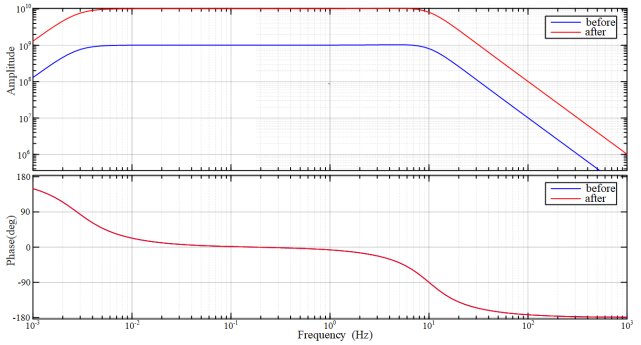

FIGURE 2. Variations in amplitude-frequency and phase-frequency responses when the sensitivity is increased by ten times. The results before and after changing the parameters are shown in blue and red, respectively.

on NCCF [17] :

$$\psi_{ij}(\mathrm{t}) = \tau(t) + \omega(\mathrm{t}) + \sigma(\mathrm{t})_{ij} \tag{2}$$

where ψ is the time offset on the positive and negative time waveform of the NCCF, τ is the time offset caused by seismograph errors, ω is the time offset caused by the physical changes, σ is the time offset caused by changes in noise sources and ij is the two components of NCCF. τ will cause the entire waveform to shift left or right (Fig. 3a), ω will cause the waveform to stretch or compress (Figs. 3b-c) and σ will affect the amplitude of the positive or negative time waveforms independently (Figs. 3d-e). The time offsets caused by seismograph errors can be separated since τ is an even function and ω is an odd function:

$$\frac{\psi_{ij}(t) + \psi_{ij}(-t)}{2} = \tau(t) + \frac{\sigma_{ij}(t) + \sigma_{ij}(-t)}{2} \tag{3}$$

As increasing the length of the time series can reduce the influence of σ, positive and negative time waveforms can be used to separate the time offset caused by seismograph errors:

$$\frac{\psi_{ij}(t) + \psi_{ij}(-t)}{2} = \tau(t) \tag{4}$$

Different decomposition and entropy methods are utilized to extract the amplitude and phase features in NCCF (Fig. 4).

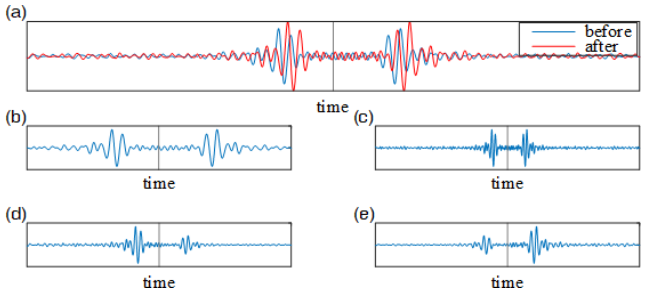

FIGURE 3. NCCF influencing factors. (a) The time offset of the entire NCCF caused by seismograph errors (the blue curve is the ideal NCCF, and the red curve is the NCCF after seismograph errors); (b-c) NCCF variations due to physical changes in the medium; (d-e) NCCF variations caused by the uneven distribution of noise sources.

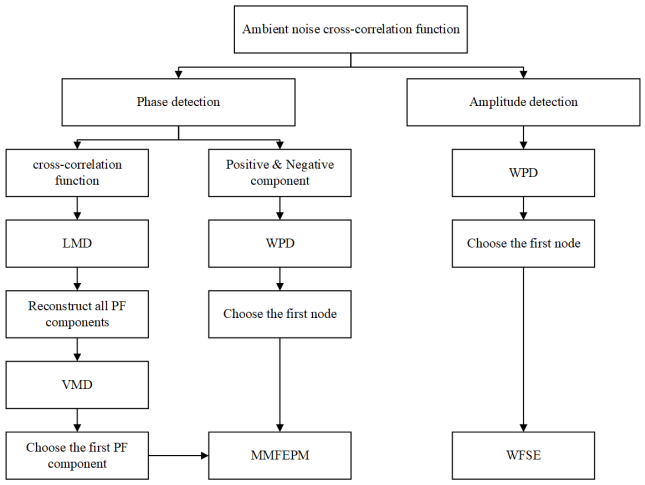

FIGURE 4. Flow chart of phase and amplitude evaluating methods.

The phase variations of the whole NCCF are evaluated using LMD-VMD-MMFEPM (Multivariable Multiscale Fuzzy Entropy Partial Mean), whereas those of positive and negative time waveforms are evaluated using WPD-MMFEPM. WPD-WFSE (Wavelet Feature Scale Entropy) is used to evaluate amplitude variations in the three waveforms. The relationships between the three waveforms can be utilized to analyze the variations induced by performance changes.

LMD is used to reduce noise interference by analyzing the local time-frequency characteristics of NCCF. The method needs first to calculate the local mean function $m_{ll}(t)$ and envelope estimation function $a_{ll}(t)$ of NCCF. Then, subtract$m_{ll}(t)$ from NCCF to obtain a new signal $x_{\text{new}}(t)$. Demodulate $x_{\text{new}}(t)$ to a pure FM signal, and then multiply all local envelope functions to get the envelope signal. The first Product Function (PF) of LMD is the product of the envelope signal and the pure FM signal, which has the highest frequency in NCCF. Repeat the previous steps until the residual is a monotone function after separating PF from NCCF:

$$x(t) = \sum_{p=1}^{k} PF_p(t) + u_k(t) \tag{5}$$

where k is the number of PF, PF_p is the pth PF, and $u_k(t)$ is the residual.

All the PFs are stacked to create a new waveform since LMD has a mode mixing problem and removing some components may cause the loss of information:

$$X(t) = \sum_{p=1}^{k} PF_p(t) \tag{6}$$

VMD is utilized to process X(t) as a secondary decomposition to reduce noise interference and avoid modal mixing. Assuming k Intrinsic Mode Functions (IMFs), the variance constraint model is as follows:

$$\begin{aligned} &\min_{\{u_k,\omega_k\}} \left\{ \sum_k \left\| \partial_t \left| (\delta(t) + \tfrac{j}{\pi t}) u_t(t) \right| e^{-j\omega_t t} \right\|_2^2 \right\} \\ &s.t. \sum_{k=1} u_k = x \end{aligned} \tag{7}$$

where $\{u_k\}$ is IMF and $\{\omega_k\}$ is the center frequency of each IMF. The constrained variational issue is changed to an unconstrained variational problem by using a penalty factor α and a Lagrange multiplier operator $\lambda(t)$:

$$\begin{aligned} &L\left(\{u_k\}, \{\omega_k\}, \lambda\right) \\ &= \alpha \sum_k \left\| \partial_t \left[(\delta(t) + j/\pi t) * u_k(t) \right] e^{-j\omega_k t} \right\|_2^2 \\ &\quad + \left\| f(t) - \sum_k u_k(t) \right\|_2^2 \\ &\quad + \left\langle \lambda(t), f(t) - \sum_k u_k(t) \right\rangle \end{aligned} \tag{8}$$

The optimal solution of the variational model and the IMFs can be obtained through iteration and optimization of u_k, ω_k and $\lambda(t)$.

MMFEPM [27], composed of MMFE and PM, is chosen to describe the phase information in IMF. Compared with other measurement methods, like Slope Entropy (SlEn) and Permutation Entropy (PE) [28], MMFE is more suitable for NCCF processing. In MMFE, coarse granulation ensures that IMF can be analyzed from multiple perspectives, and the fuzzy membership function $K(x)$ has a significant impact on the statistical stability of the MMFE entropy values. They ultimately make the calculation results more reflective of the phase variations of the waveforms. When the Chebyshev distance $d\left[Y_m(i), Y_m(j)\right] \in [0, r]$, write $K(x)$ as M_i and when $d\left[Y_m(i), Y_m(j)\right] > r$, write $K(x)$ as N_i, where r is the given threshold value. Let $E_i = M_i + N_i$ and the frequency of E_i is $L_i^m(r)$. The MMFE can be written as follows:

$$IMSE\left(M, \lambda, r, N\right) = -ln\left[\frac{L^{m+1}(r)}{L^m(r)}\right] \tag{9}$$

PM is used to analyze the central trend of MMFE values under different scale factors:

$$H_{mp}^{pe} = \left(1 + \left|\frac{S_{ke}}{3}\right|\right) \times H_{mp}^{m} \tag{10}$$

where S_{ke} is the skewness and H_{mp}^{m} is the entropy mean.

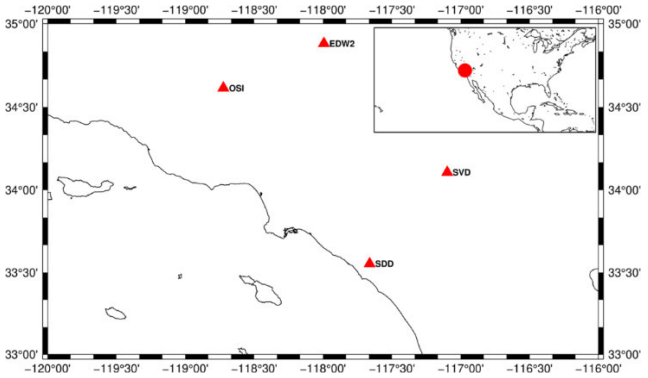

FIGURE 5. Map of the study area. The stations are indicated by triangles with station names beside each symbol. The inset shows the location of stations on the larger map.

WPD is used to filter the positive and negative time waveforms at high and low frequencies, resulting in the wavelet node. The phase information in the wavelet node can be evaluated using the MMFEPM value.

Noise sources and other interference factors can influence the amplitude of NCCF. These three waveforms are processed using WPD as well, and the WFSE values are then calculated to describe the amplitude information. The measure of the wavelet coefficients $d_j(k)$ is determined as follows:

$$p_{jk} = \frac{d_{Fj}(k)}{\sum_{k=1}^{N} d_{F(j)}(k)} \tag{11}$$

where $d_{F(j)}(k)$ is the Fourier transform of $d_j(k)$. The WFSE value is defined by the information entropy:

$$W_{FSE_j} = -\sum_{k=1}^{N} P_{jk} log P_{jk} \tag{12}$$

where W_{FSE_j} is the WFSE value of the jth scale of the sequence.

III. DATA AND RESULTS

A. DATA PROCESSING

The seismic ambient noise data from the CI network in the Los Angeles Basin region of Southern California from September to December 2006 is selected (Fig. 5). Following data preprocessing [29], the raw data with a frequency of 40Hz is filtered in the 0.01-0.1Hz band and then divided into one-hour time windows to calculate the daily NCCF. The NCCF can be obtained by stacking the daily NCCF with correlation coefficients greater than 0.4 for different days [30], and then evaluating the phase and amplitude variations within the ±125s time window (Fig. 6).

The whole NCCF is shifted (Fig. 7a) to simulate different phase variations in the range of 0.025 to 2.5s and the waveform is multiplied by different coefficients to simulate small variations in amplitude (Fig. 7b).

B. RESULTS OF PHASE EVALUATING

NCCF is processed with LMD to obtain four PFs and one residual component. The waveform tends to be monotonous as the number of PF increases. Stack all PFs to get a new

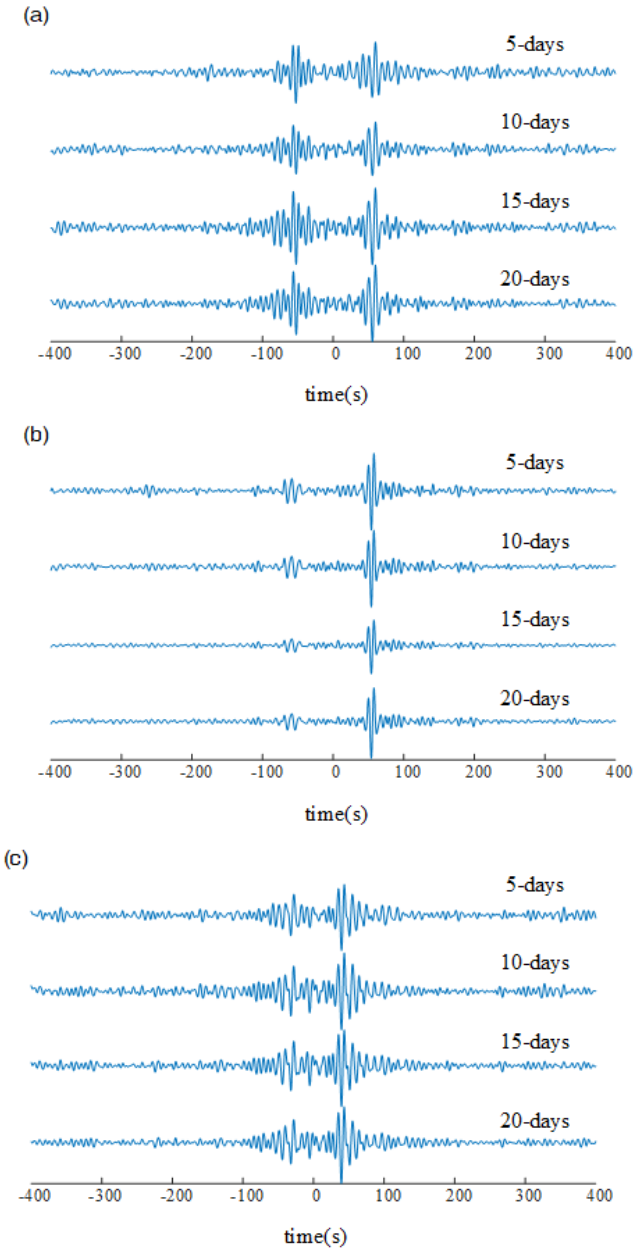

FIGURE 6. NCCFs of (a) OSI-SDD, (b) OSI-SVD, and (c) EDW2-SVD station pairs for different stacking days.

waveform X (t) to avoid the loss of information and then use VMD to further analyze the waveform. The number of IMFs is set to two. Positive and negative time waveforms can be distinguished from IMF1 (Fig. 8) and the correlation coefficient with X (t) is higher than that with IMF2 and X(t). Therefore, the IMF1 that maintains more phase information is selected for further processing.

The MMFEPM value of IMF1 is calculated to describe phase information from different scales. The MMFEPM value of the OSI-SDD station pair decreases monotonically as the time offset increases from 0.025s to 2.5s (Figs. 9a and 9b). According to the results of the EDW2-SVD and OSI-SVD station pairs (Figs. 9c and 9d), as well as the OSI-SDD station pair, this method can be applied to evaluate NCCFs in different directions and distances.

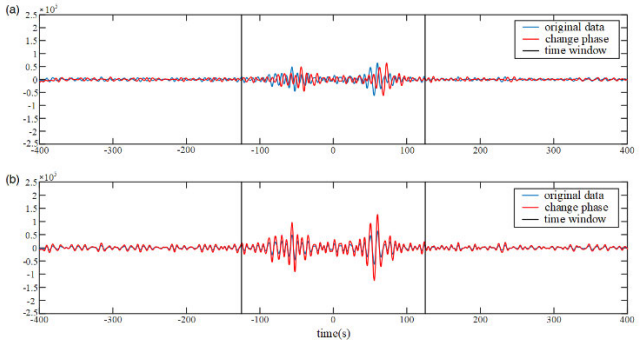

FIGURE 7. Simulation of the phase and amplitude variations of the NCCF due to the seismograph performance, the selected waveforms are contained within the solid black line. (a) Shifting the waveform by 500 points (12.5s); (b) Multiplying the amplitude of the waveform by a factor of two.

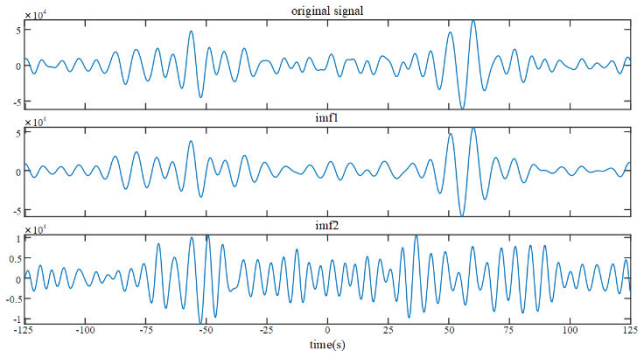

FIGURE 8. Results of VMD.

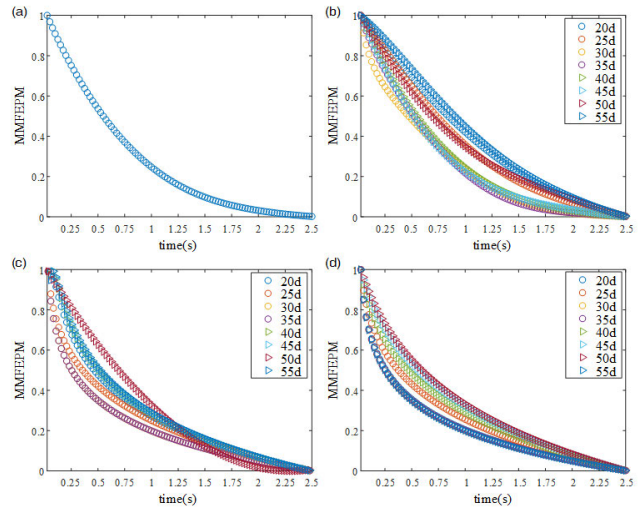

FIGURE 9. The phase evaluation results of different station pairs (normalized). (a) Variations in MMFE values as the time offsets increase (single NCCF of OSI-SDD station pair); (b) Variations in MMFE values as the time offsets increase (NCCFs for different stacking days of OSI-SDD station pair); (c) The same as (b), but of the EDW2-SVD station pair; (d) The same as (b), but of the OSI-SVD station pair.

A four-layer WPD is used to process the positive and negative time waveforms. Since the nodes are arranged from low to high frequency, the first node is chosen to calculate the MMFEPM value. The MMFE values of these two waveforms increase initially and subsequently decrease as the time offsets increase (Fig. 10). The evaluation range of

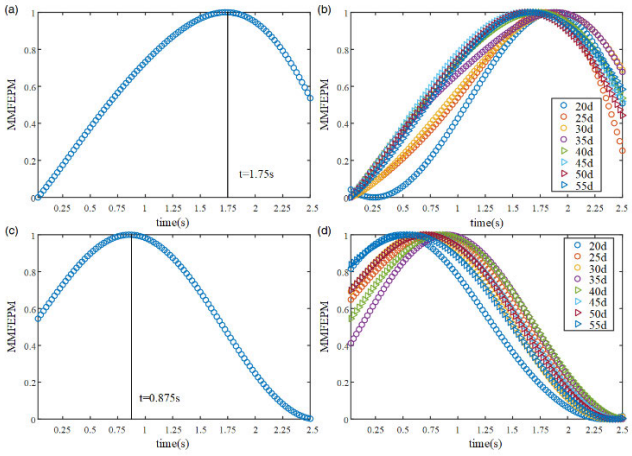

FIGURE 10. The phase evaluation results of positive and negative time waveforms of the OSI-SDD station pair (normalized). (a) The result of a single positive-time waveform; (b) The results of the positive-time waveform for different stacking days; (c) The result of a single negative-time waveform; (d) The results of the negative-time waveform for different stacking days. The black solid lines are the evaluation ranges.

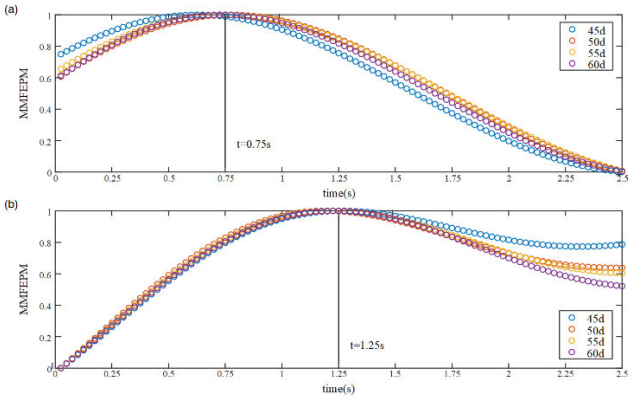

FIGURE 11. The phase evaluation results of (a) positive and (b) negative time waveforms of the EDW2-SVD station pair for different stacking days (normalized). The black solid lines are the evaluation ranges.

the positive time waveform is larger than that of the negative time waveform (the rising part is taken as the evaluation range). The higher the waveform energy, the wider the evaluation range. This conclusion can be confirmed by comparing the evaluation ranges of three waveforms of the EDW2-SVD station pair (Fig. 11).

C. RESULTS OF AMPLITUDE EVALUATING

Since interference factors can easily impact the amplitude of NCCF, it is important to properly identify amplitude variations caused by changes in seismograph performance. The influence of physical medium change can be avoided by improving time resolution as it is not easy to change in a short time and has little impact on the waveform. Therefore, the amplitude variations caused by performance changes can be determined by separating the effect of the noise source.

Set the sliding windows with a duration of 40 days and a step of 1 day to calculate the NCCF of the OSI-SDD station pair (Fig. 12) and take the amplitude in the first time window as a reference. The influence of noise sources can

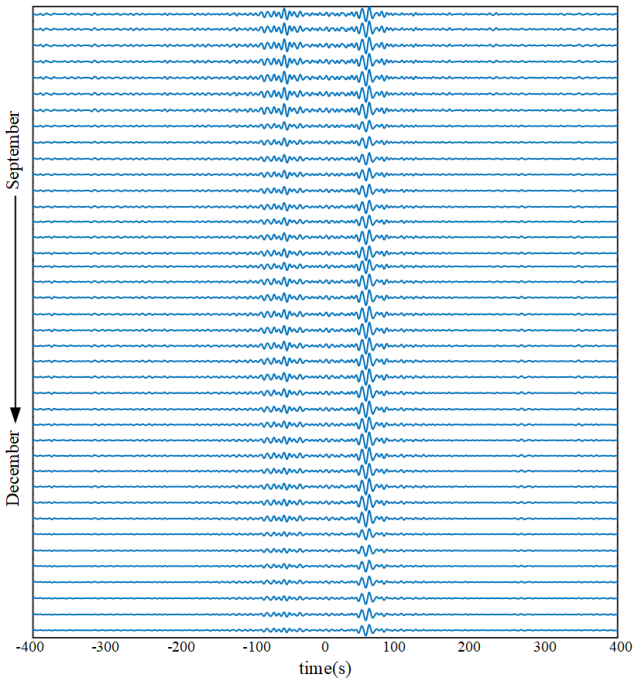

FIGURE 12. Variations of noise sources over time.

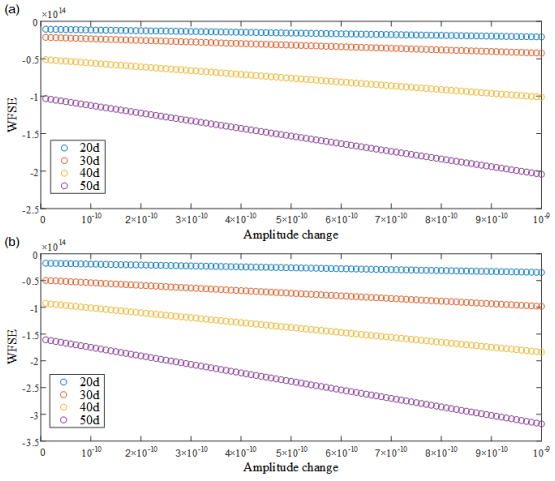

FIGURE 13. The amplitude evaluation results of NCCFs. (a) The results of the OSI-SDD station pair for different stacking days; (b) The same as (a), but of the OSI-SVD station pair.

be separated by calculating the WFSE values of two NCCFs and subtracting the difference in the values between two adjacent time windows from the WFSE value of the latter time window.

A three-layer WPD is utilized to analyze the amplitude variations of NCCF, and the first node is selected to calculate the WFSE value. The WFSE values of the OSI-SDD station pair for different stacking days decrease monotonically with increasing amplitude (Fig. 13a). When the amplitude changes are the same, the absolute value of WFSE increases with increasing SNR. The results of the OSI-SVD station pair verify the practicality of this method (Fig. 13b).

The amplitude of positive and negative time waveforms is evaluated using the same method as NCCF. The results of the OSI-SDD station pair for different stacking days

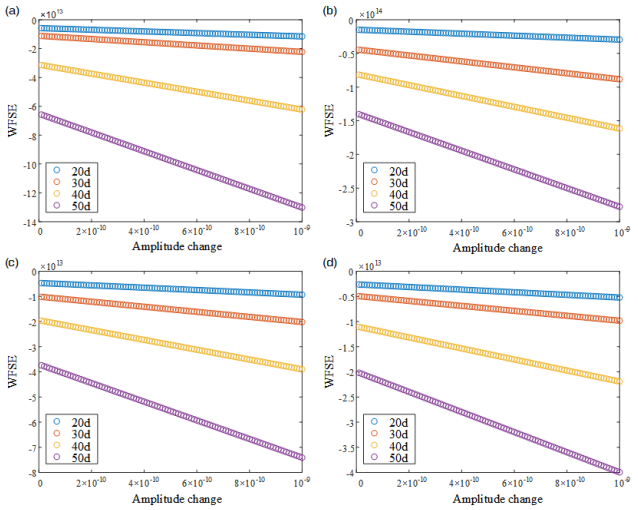

FIGURE 14. The amplitude evaluation results of positive and negative-time waveforms. (a) The results of the positive time waveform of the OSI-SDD station pair for different stacking days; (b) The same as (a), but of the OSI-SVD station pair; (c) The results of the negative time waveform of the OSI-SDD station pair for different stacking days; (d) The same as (c), but of the OSI-SVD station pair.

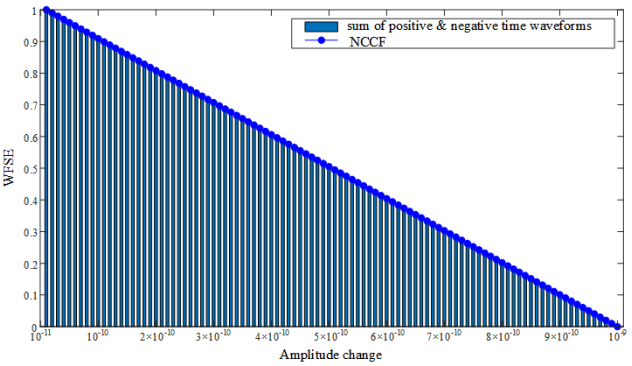

FIGURE 15. The relationships between the WFSE values of the NCCF of the OSI-SDD station pair and the sum of the WFSE values of the positive and negative time waveforms(normalized).

show a monotonic decreasing trend with increasing amplitude (Figs. 14a and 14c). The higher the waveform energy, the larger the absolute value of WFSE. The WFSE value of NCCF is equal to the sum of WFSE values of positive and negative time waveforms (Fig. 15). These conclusions are validated by the amplitude evaluation results of OSI-SVD stations (Figs. 14b and 14d).

IV. METHOD VERIFICATION

To calculate the NCCFs and confirm the reliability of the phase and amplitude evaluation methods, data from the OSI-SDD station pair between September and December 2006 is chosen. A sliding window with a period of 40 days and a step of 1 day is then defined.

A. THE VERIFICATION OF THE PHASE EVALUATING METHOD

The MMFEPM values of all the original waveforms (written as the original result) are first calculated, then the phase is changed in a certain time window to calculate the MMFEPM value (written as the changed result). The validity of the

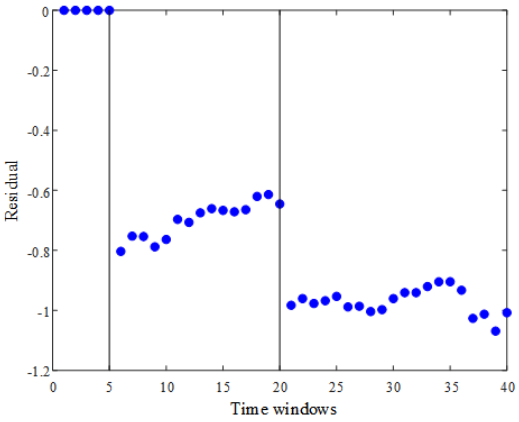

FIGURE 16. Residuals between the original and final results of the OSI-SDD station pair, where the black solid lines are the fifth and twentieth time windows, respectively.

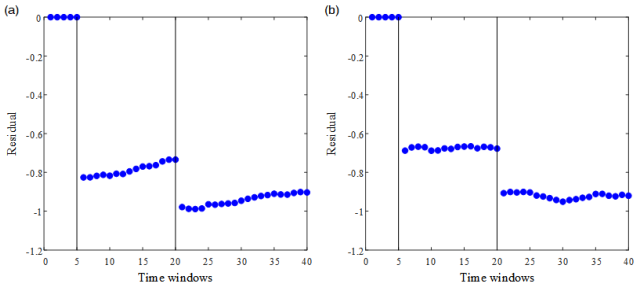

FIGURE 17. Residuals between the original and final results of the (a) positive and (b) negative time waveforms of the OSI-SDD station pair, where the black solid lines are the fifth and twentieth time windows, respectively.

method can be verified by comparing the residuals between the original and changed results in the same time window.

The MMFEPM values of all time windows are recorded as the original results. The waveforms are then shifted by 10 points (0.25s) in the sixth to twentieth time windows and 25 points (0.625s) in the twenty-second to fortieth time window (recorded as the initial results). To better assess the unity of the results, the initial results are divided by the PM value of the period (recorded as the final results). The residuals between the original and the final results show breakpoints in the fifth and twentieth time windows (Fig. 16), indicating that this method can evaluate the phase variations in NCCF.

The changed time windows and phases of positive and negative time waveforms are consistent with the above. Breakpoints are visible in the fifth and twentieth time windows (Fig. 17), demonstrating that this method can identify the phase variations in both positive and negative time waveforms.

It's essential to evaluate whether the variations of the three waveforms are the same. We first need to find the MMFEPM value of the changed phase (written as evaluation result) and then shift this waveform within 0.025-2.5s (written as simulation result). When the MMFEPM values between the two results are the closest, the evaluation result has the same time offset as the simulation result. The three waveforms in these two periods all have the same time offsets of 0.25s and

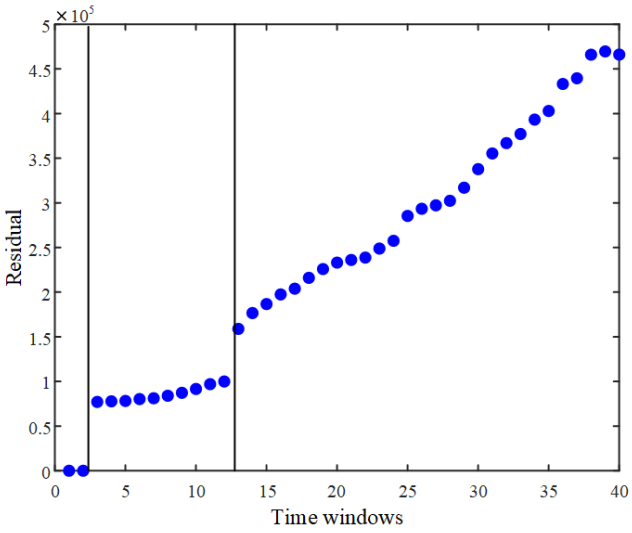

FIGURE 18. The residuals between the original and changed results of the NCCF, where the black solid lines are the second and thirteenth time windows, respectively.

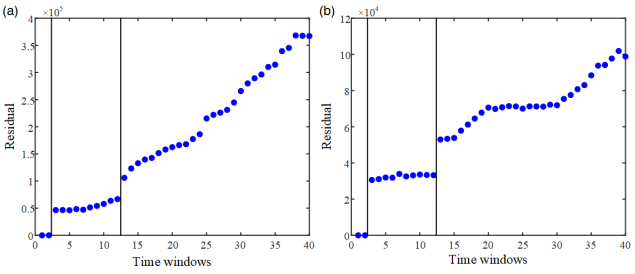

FIGURE 19. The residuals between the original and changed results of the (a) positive and (b) negative time waveforms, where the black solid lines are the second and thirteenth time windows, respectively.

0.625s, proving that the phase variations are caused by the performance change.

B. THE VERIFICATION OF THE AMPLITUDE EVALUATING METHOD

The WFSE value of the waveform requires to be calculated after separating the influence of the noise source (recorded as the original result). After that, change the amplitude in a certain time window and calculate the WFSE value (recorded as the changed result). The reliability of the amplitude evaluation method can be demonstrated by comparing the residuals between the original and changed results.

From the third to the twentieth and the thirteenth to the fortieth time window, the amplitudes of the waveforms are multiplied by $6.7 \times 10^{-10}$and 10^{-9}, respectively. Breakpoints in the residuals between the original and changed results are found in the second and thirteenth time windows (Fig. 18), indicating that this method can identify amplitude variations.

The changed time windows and amplitude of positive and negative time waveforms are consistent with the preceding. The breakpoints appear in the second and thirteenth time windows (Fig. 19), indicating that this method can assess the amplitude variations in positive and negative time waveforms.

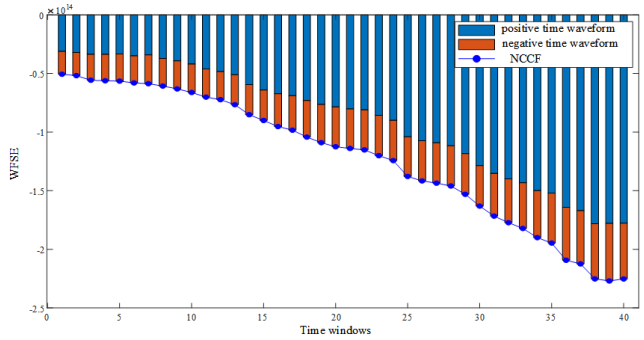

FIGURE 20. The relationships between the WFSE value of the NCCF and the sum of the WFSE values of the positive and negative time waveforms.

The WFSE value of the changed amplitude is recorded as the evaluation result. The WFSE values for this amplitude range are then calculated using the slope (written as simulation data). When the WFSE values are closest, the amplitude variation of the simulation data is the same as that of the evaluation data. The amplitude variations of the three waveforms in these two periods are 6.7×10^{-10} and 10^{-9} , showing that the amplitude variations are caused by performance change. This conclusion is further supported by the fact that the WFSE value of NCCF is equal to the sum of the WFSE values of positive and negative time waveforms (Fig. 20).

We multiply the amplitudes of the three waveforms by 1.6×10^{-10} and 3.0×10^{-10} in the eighth to twenty-first and twenty-second to fortieth time windows, respectively. All waveforms have breakpoints in the eighth and twenty-second time windows (Figs. 21a-c). By comparing the WFSE values of the three waveforms, it is confirmed that the amplitude variation is caused by changes in seismograph performance (Fig. 21d). Furthermore, the amplitude range is $10^{-11} - 10^{-9}$ both in the eighth to twenty-first and twenty-second to fortieth time windows. The amplitude variations in the corresponding time windows of the three waveforms are the same by comparing the simulation and evaluation results. It is further proved that by analyzing the relationships between the WFSE values of the three waveforms, it is possible to determine whether the amplitude variations are caused by performance changes.

V. CONCLUSION

We propose to use the features of NCCF as well as positive and negative time waveforms to monitor the performance of seismographs online.

LMD-VMD-MMFEPM is utilized to evaluate the phase variations of the entire NCCF and the time offsets within 0.025-2.5s can be identified. WPD-MMFEPM is then used to evaluate the phase variations of positive and negative time waveforms. Since the evaluation range is decided by the smallest of the three waveforms, selecting the station pairs whose positive and negative time waveforms are more evenly affected by noise source can obtain a wider range. It is necessary to separate the influence of the noise source since it has an independent impact on both the positive and negative time waveforms. The smallest variation in amplitude of the three waveforms that can be evaluated using WPD-WFSE is 10^{-16}. Distance and azimuth do not affect the evaluation accuracy.

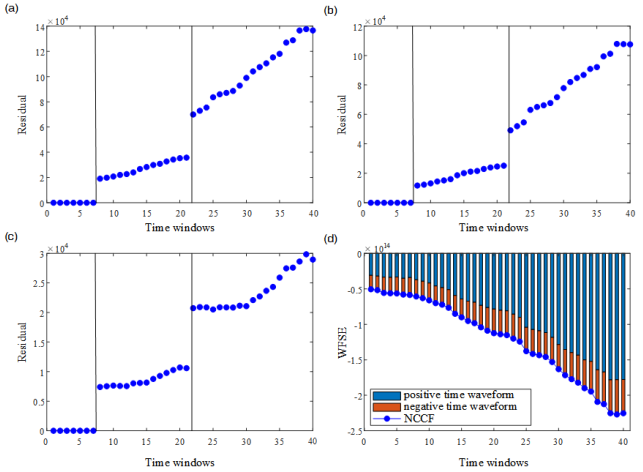

FIGURE 21. The evaluation results among the NCCF, positive and negative time waveforms. (a) Residuals of the WFSE values between the original and changed results of NCCF; (b) The same as (a), but of positive time waveform; (c) The same as (a), but of negative time waveform; (d) The relationships between the WFSE values of the three waveforms. The black solid lines are the eighth and twenty-second time windows, respectively.

The proposed feature extraction methods can test the small variations in the ambient noise waveform and swiftly evaluate the performance of the seismograph. Following that, the combination of this method and machine learning can realize the automatic detection and early warning of the performance of the seismograph, thereby promoting the intelligent application of the seismograph.

ACKNOWLEDGMENT

The authors would like to thank iris (https://www.iris.edu) for the data and the reviewers for their constructive reviews.

REFERENCES

[1] C. R. Hutt and A. T. Ringler, "Some possible causes of and corrections for STS-1 response changes in the global seismographic network," *Seismolog. Res. Lett.*, vol. 82, no. 4, pp. 560–571, Jul. 2011, doi: 10.1785/gssrl.82.4.560.

[2] C. D. Doody, A. T. Ringler, R. E. Anthony, D. C. Wilson, A. A. Holland, C. R. Hutt, and L. D. Sandoval, "Effects of thermal variability on broadband seismometers: Controlled experiments, observations, and implications," *Bull. Seismolog. Soc. Amer.*, vol. 108, no. 1, pp. 493–502, Feb. 2018, doi: 10.1785/0120170233.

[3] J. Lin, H. Gao, X. Wang, C. Yang, Y. Xin, and X. Zhou, "Effect of temperature on the performance of electrochemical seismic sensor and the compensation method," *Measurement*, vol. 155, Apr. 2020, Art. no. 107518, doi: 10.1016/j.measurement.2020.107518.

[4] K. Aderhold, K. E. Anderson, A. M. Reusch, M. C. Pfeifer, R. C. Aster, and T. Parker, "Data quality of collocated portable broadband seismometers using direct burial and vault emplacement," *Bull. Seismolog. Soc. Amer.*, vol. 105, no. 5, pp. 2420–2432, Oct. 2015, doi: 10.1785/0120140352.

[5] C. R. Hutt, A. T. Ringler, and L. S. Gee, "Broadband seismic noise attenuation versus depth at the albuquerque seismological laboratory," *Bull. Seismolog. Soc. Amer.*, vol. 107, no. 3, pp. 1402–1412, Jun. 2017, doi: 10.1785/0120160187.

[6] K. Smith and C. Tape, "Seismic noise in central Alaska and influences from rivers, wind, and sedimentary basins," *J. Geophys. Res. B, Solid Earth Planets.*, vol. 124, no. 11, pp. 678–704, 2019, doi: 10.1029/2019JB017695.

[7] S. De Angelis and P. Bodin, "Watching the wind: Seismic data contamination at long periods due to atmospheric pressure-field-induced tilting," *Bull. Seismolog. Soc. Amer.*, vol. 102, no. 3, pp. 1255–1265, Jun. 2012, doi: 10.1785/0120110186.

[8] S. N. Dybing, A. T. Ringler, D. C. Wilson, and R. E. Anthony, "Characteristics and spatial variability of wind noise on near-surface broadband seismometers," *Bull. Seismolog. Soc. Amer.*, vol. 109, no. 3, pp. 1082–1098, Jun. 2019, doi: 10.1785/0120180227.
[9] P. Davis, M. Ishii, and G. Masters, "An assessment of the accuracy of GSN sensor response information," *Seismol. Res. Lett.*, vol. 77, no. 2, p. 159, 2006.
[10] T. Kimura, H. Murakami, and T. Matsumoto, "Systematic monitoring of instrumentation health in high-density broadband seismic networks," *Earth, Planets Space*, vol. 67, no. 1, pp. 1–15, Dec. 2015, doi: 10.1186/s40623-015-0226-y.
[11] A. T. Ringler, R. E. Anthony, C. A. Dalton, and D. C. Wilson, "Rayleigh-wave amplitude uncertainty across the global seismographic network and potential implications for global tomography," *Bull. Seismolog. Soc. Amer.*, vol. 111, no. 3, pp. 1273–1292, Mar. 2021, doi: 10.1785/0120200255.
[12] D. E. McNamara, C. R. Hutt, L. S. Gee, H. M. Benz, and R. P. Buland, "A method to establish seismic noise baselines for automated station assessment," *Seismolog. Res. Lett.*, vol. 80, no. 4, pp. 628–637, Jul. 2009, doi: 10.1785/gssrl.80.4.628.
[13] S. J. Rastin, C. P. Unsworth, K. R. Gledhill, and D. E. McNamara, "A detailed noise characterization and sensor evaluation of the north island of new Zealand using the PQLX data quality control system," *Bull. Seismolog. Soc. Amer.*, vol. 102, no. 1, pp. 98–113, Feb. 2012, doi: 10.1785/0120110064.
[14] E. Wolin and D. E. McNamara, "Establishing high-frequency noise baselines to 100 Hz based on millions of power spectra from IRIS MUSTANG," *Bull. Seismolog. Soc. Amer.*, vol. 110, no. 1, pp. 270–278, Feb. 2020, doi: 10.1785/0120190123.
[15] Z. Li, E. Hauksson, and J. Andrews, "Methods for amplitude calibration and orientation discrepancy measurement: Comparing co-located sensors of different types in the southern California seismic network," *Bull. Seismolog. Soc. Amer.*, vol. 109, no. 4, pp. 1563–1570, Aug. 2019, doi: 10.1785/0120190019.
[16] W. Xu, D. Yang, S. Yuan, J. Ma, J. Xie, and X. Li, "Calculation of the sensitivity of the in-situ seismograph using the collocation test," *Chin. J. Geophys.*, vol. 64, no. 12, pp. 4572–4581, 2021, doi: 10.6038/cjg2021P0457.
[17] L. Stehly, M. Campillo, and N. M. Shapiro, "Traveltime measurements from noise correlation: Stability and detection of instrumental time-shifts," *Geophys. J. Int.*, vol. 171, no. 1, pp. 223–230, Oct. 2007, doi: 10.1111/j.1365-246X.2007.03492.x.
[18] C. Sens-Schönfelder, "Synchronizing seismic networks with ambient noise," *Geophys. J. Int.*, vol. 174, no. 3, pp. 966–970, Sep. 2008, doi: 10.1111/j.1365-246X.2008.03842.x.
[19] F. Ye, J. Lin, Z. Shi, and S. Lyu, "Monitoring temporal variations in instrument responses in regional broadband seismic network using ambient seismic noise," *Geophys. Prospecting*, vol. 66, no. 5, pp. 1019–1036, Jun. 2018, doi: 10.1111/1365-2478.12621.
[20] J. Yu and Z. Zhang, "Research on the seismic signal denoising with the LMD and EMD method," in *Proc. IEEE 2nd Adv. Inf. Technol., Electron. Autom. Control Conf. (IAEAC)*, Mar. 2017, pp. 767–771, doi: 10.1109/IAEAC.2017.8054119.
[21] W. Liu, S. Cao, and Z. Wang, "Application of variational mode decomposition to seismic random noise reduction," *J. Geophys. Eng.*, vol. 14, no. 4, pp. 888–899, Aug. 2017, doi: 10.1088/1742-2140/aa6b28.
[22] E. Proano, D. S. Benitez, R. Lara-Cueva, and M. Ruiz, "On the use of variational mode decomposition for seismic event detection," in *Proc. IEEE Int. Autumn Meeting Power, Electron. Comput. (ROPEC)*, Nov. 2018, pp. 1–6, doi: 10.1109/ROPEC.2018.8661428.
[23] D. Long, C. Niu, H. L. Zhou, R. Huang, and W. Zhou, "Application of VMD algorithm in time-frequency analysis of seismic data," *Prog. Geophys.*, vol. 35, no. 1, pp. 166–173, 2020, doi: 10.6038/pg2020CC0462.
[24] G. Li, W. Chang, and H. Yang, "A new hybrid model for underwater acoustic signal prediction," *Complexity*, vol. 2020, pp. 1–19, Jul. 2020, doi: 10.1155/2020/5167469.
[25] Y. Li, B. Tang, and Y. Yi, "A novel complexity-based mode feature representation for feature extraction of ship-radiated noise using VMD and slope entropy," *Appl. Acoust.*, vol. 196, Jul. 2022, Art. no. 108899, doi: 10.1016/j.apacoust.2022.108899.
[26] H. Chai, H. Huang, Z. Yan, X. Zhang, Y. Li, P. Gan, and Y. Huang, "Multi-threshold wavelet packet-based method to attenuate noise from seismic signal," in *Proc. 7th Int. Conf. Informat., Environ., Energy Appl. (IEEA)*, 2018, pp. 212–216, doi: 10.1145/3208854.3208876.
[27] M. Ahmed, T. Chanwimalueang, S. Thayyil, and D. Mandic, "A multivariate multiscale fuzzy entropy algorithm with application to uterine EMG complexity analysis," *Entropy*, vol. 19, no. 1, p. 2, Dec. 2016, doi: 10.3390/e19010002.
[28] Y. Li, P. Gao, B. Tang, Y. Yi, and J. Zhang, "Double feature extraction method of ship-radiated noise signal based on slope entropy and permutation entropy," *Entropy*, vol. 24, no. 1, p. 22, Dec. 2021, doi: 10.3390/e24010022.
[29] G. D. Bensen, "Processing seismic ambient noise data to obtain reliable broad-band surface wave dispersion measurements," *Geophys. J. Int.*, vol. 169, no. 3, pp. 1239–1260, 2007, doi: 10.1111/j.1365-246X.2007.03374.x.
[30] K. Løviknes, "Measuring seismic station timing errors from ambient noise," M.S. thesis, Dept. Earth Sci., Univ. Bergen, Bergen, Norway, 2018.

XUE BAO received the bachelor's degree in communication engineering. She is currently pursuing the master's degree in instrument science and technology with China Jiliang University. Her research interests include seismic science and instruments, instrument testing and measurement, industrial data acquisition and processing, machine learning, and artificial intelligence.

FANG YE received the bachelor's and master's degrees in electronic information engineering, and the Ph.D. degree in measurement technology and instrument from Jilin University. She is currently a Teacher in measurement and control technology and instrument with China Jiliang University. Her research interests include seismic science and instruments, instrument testing and measurement, industrial data acquisition and processing, machine learning, and artificial intelligence.

HAN ZHANG received the bachelor's degree in measurement technology and instrument from China Jiliang University, where she is currently pursuing the Graduate degree in measurement and control technology and instrument. Her research interests include seismic science and instruments, instrument testing and measurement, industrial data acquisition and processing, machine learning, and artificial intelligence.

CHUNWEI JIN received the bachelor's degree in measurement & control technology and instrument from China Jiliang University, where he is currently pursuing the master's degree in instrument science and technology. His research interests include seismic data processing, instrument science, artificial intelligence, and deep learning.